

Imaging the seismic structure of the crust and upper mantle beneath the Great Plains, Rio Grande Rift, and Colorado Plateau using receiver functions

David Wilson,^{1,2} Richard Aster,¹ James Ni,³ Stephen Grand,⁴ Michael West,³ Wei Gao,⁴ W. Scott Baldrige,⁵ and Steve Semken⁶

Received 20 October 2004; accepted 2 March 2005; published 28 May 2005.

[1] The seismic structure of the crust and upper mantle of the southwestern United States is examined using receiver functions calculated from teleseismic arrivals recorded in the Colorado Plateau–Rio Grande Rift–Great Plains Seismic Transect (LA RISTRA) experiment. We apply receiver function estimation and filtering methods developed by Wilson and Aster (2005) to produce receiver functions with decreased sensitivity to noise and deconvolutional instability. Crustal thickness and V_p/V_s ratios are estimated using both direct and reverberated P -to- S receiver function modes. We apply regularized receiver function migration methods to produce a multiple-suppressed image of the velocity discontinuity structure of the subsurface. Our results show that crustal thickness averages 44.1 ± 2.3 km beneath the Great Plains (GP) and 45.6 ± 1.1 km beneath the Colorado Plateau (CP). Crustal thinning beneath the Rio Grande Rift (RGR) is broadly symmetric about the rift axis, with the thinnest crust (35 km) located directly beneath the rift axis, suggesting a pure shear stretched lithosphere beneath the RGR. We also observe a prominent northwest dipping discontinuity, ranging from 65 to 85 km deep beneath the CP, and possible subcrustal discontinuities beneath the GP. These discontinuities, along with recent xenolith data, are consistent with preserved ancient lithospheric structures such as relict suture zones associated with Proterozoic subduction. We observe an upper mantle discontinuity at 220–300 km depth that may correlate with similar discontinuities observed beneath eastern North America. We also observe relatively flat discontinuities at 410 and 660 km depth, indicating there is not a large-scale thermal anomaly beneath the RGR at these depths.

Citation: Wilson, D., R. Aster, J. Ni, S. Grand, M. West, W. Gao, W. S. Baldrige, and S. Semken (2005), Imaging the seismic structure of the crust and upper mantle beneath the Great Plains, Rio Grande Rift, and Colorado Plateau using receiver functions, *J. Geophys. Res.*, 110, B05306, doi:10.1029/2004JB003492.

1. Introduction

[2] The crustal basement of the Colorado Plateau–Rio Grande Rift–Great Plains Seismic Transect (LA RISTRA) region in the southwestern United States (Figure 1) was assembled in a series of continent building events where

Proterozoic terranes, generally consisting of an assemblage of island arcs, oceanic plateaus, and marginal basin units [Condie, 1986; Condie and Selverstone, 1999; Frey *et al.*, 2001], were accreted to the continent, younging to the southeast [Condie, 1982; Bowring and Karlstrom, 1990]. The RISTRA experiment was oriented approximately parallel to this regional Proterozoic accretionary gradient, crossing two major Proterozoic province boundaries, the Mazatzal and Yavapai provinces (1.6–1.7 Ga and 1.7–1.8 Ga, respectively) in the northwestern portion of the array and the ≈ 1.1 Ga Grenville province boundary near the edge of the Delaware basin in the southeast [Condie, 1982; Bowring and Karlstrom, 1990]. There is also evidence for up to three periods of Proterozoic continental extension and rifting [Marshak and Paulsen, 1996]. The first extensional episode was northeast-southwest at 1.5–1.3 Ga, followed by east-west to northwest-southeast extension at 1.1 Ga in conjunction with the Grenville orogeny, and east-west extension at 0.7–0.6 Ga. Regional basement-penetrating faults formed during this time may have created long-lived zones of crustal weakness which affected the style of

¹Department of Earth and Environmental Science and Geophysical Research Center, New Mexico Institute of Mining and Technology, Socorro, New Mexico, USA.

²Now at Department of Geological Sciences, University of Texas at Austin, Austin, Texas, USA.

³Department of Physics (MSC 3D), New Mexico State University, Las Cruces, New Mexico, USA.

⁴Department of Geological Sciences, University of Texas at Austin, Austin, Texas, USA.

⁵Earth and Environmental Sciences Division, Los Alamos National Laboratory, Los Alamos, New Mexico, USA.

⁶Department of Geological Sciences, Arizona State University, Tempe, Arizona, USA.

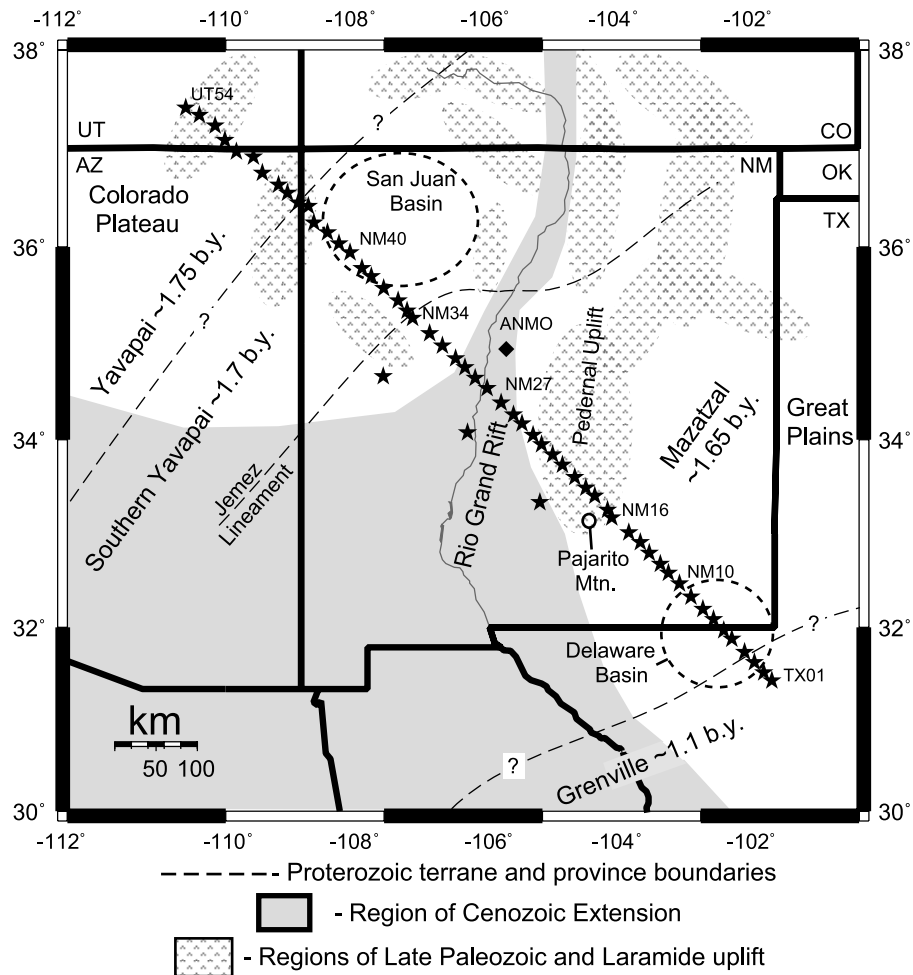


Figure 1. Regional tectonic setting of RISTRA, compiled from *Baldrige et al.* [1991], *Bowring and Karlstrom* [1990], *Reed et al.* [1993], and *Sloss* [1988].

subsequent Paleozoic crustal deformation [*Marshak et al.*, 2000].

[3] During the Pennsylvanian to Early Permian Ouachita-Marathon orogeny (320–280 Ma), a complex intraplate response associated with the collision between North America and South America–Africa resulted in the uplift of the Ancestral Rocky mountains [*Kluth and Coney*, 1981]. During the Mesozoic Laramide (80–50 Ma) orogeny the region underwent compression as the Farallon slab was subducting along the North American west coast. Crustal deformation in the Laramide was characterized by fault-bounded, basement-cored uplifts separated by intervening sediment-filled basins. During this period the Farallon slab may have been subducting at a low angle [e.g., *Dickinson and Snyder*, 1978] leading to suppressed subduction-related magmatism. Between approximately 43 to 30 Ma the flattened Farallon slab is thought to have detached and rolled back, with accompanying mantle upwelling being the controlling factor for the space-time evolution of widespread mid-Tertiary “ignimbrite flare-up” volcanism [e.g., *Dickinson and Snyder*, 1978; *Lipman et al.*, 1971; *Humphreys*, 1995]. During the interval 30–19 Ma in the middle Colorado Plateau, potassic lamprophyric eruptions of the Navajo volcanic field occurred along Laramide monoclines [*Selverstone et al.*, 1999].

[4] During the past 30 Myr the RISTRA region has undergone general tectonic extension, along with much of interior western North America. This extension has led to the creation of the Rio Grande Rift (RGR) but has left the Colorado Plateau relatively undeformed. The RGR is thought to have formed in at least two stages. An initial stage at 30 to 20 Ma, associated with low-angle faulting and crustal doming, may have been a result of upper mantle asthenospheric upwelling and thermal lithosphere erosion [*Seager and Morgan*, 1979; *Morgan et al.*, 1986; *Olsen et al.*, 1987]. After perhaps 10 Myr of relative quiescence, rift activity resumed with high-angle normal faulting and alkalic basaltic volcanism [e.g., *Baldrige et al.*, 1991]. During the past 4 Myr there has been increased volcanism along the Jemez Lineament (Figure 1), including the Mount Taylor region and (where the Jemez Lineament and western RGR boundary intersect) Jemez Mountains. The RISTRA region thus encompasses lithospheric structures that have been influenced by Proterozoic through recent tectonic events. A major challenge in such studies is to distinguish features that may have been formed as early as the age of regional crustal formation from those that may be due to geologically recent or ongoing tectonics. Furthermore, ancient and recent processes may be intimately associated in seismic images via the reactivation of preexisting struc-



Figure 2. Global distribution of the 84 earthquakes (diamonds) with $m_b \geq 5.6$, used for calculating the 2706 receiver functions used in this study. The events are teleseisms from epicentral distances of $35\text{--}95^\circ$, with great circle paths that are $\pm 10^\circ$ of the mean array azimuth. The RISTRA seismometer deployment (Figure 1) is depicted as great circle swath.

tures by thermal, lithospheric transmitted stress, or other processes.

2. RISTRA Data Set

[5] RISTRA was designed to study the crust and mantle beneath the southwestern U.S. utilizing 18 months of 20 sample/s, continuous broadband data. Broadband recorders in shallow vaults were deployed along a 950.7-km-long line consisting of 54 sites with 18 ± 3.6 km interstation station spacing, aligned approximately to a great circle between Lake Powell, Utah, and Pecos, Texas. Three additional off-line stations deployed parallel to and southwest of the main network (Figure 1) are not considered in this study. All sites were configured with Streckeisen STS-2 (120 s) seismometers and RefTek 24-bit recording data acquisition systems (models 72A-07 and 72A-08). Seismometers were installed on 10-cm-thick concrete pads in shallow (approximately 1-m-deep) vaults. Up to 0.4 m of dirt was mounded on top of each vault to reduce noise by providing further insulation and thermal mass. Power systems consisted of two 30 W solar panels and approximately 110 A hours of lead-acid battery capacity. RISTRA was oriented to take joint advantage of the geometry of the geologic basement (see above), and of back azimuths to prolific teleseismic source zones in western South America and the northeast Pacific. Deployment occurred in July–November 1999, and the last station was removed from the field in May 2001. During the deployment period 285 earthquakes with $m_b \geq 5.6$ were recorded with suitable offsets ($35\text{--}95^\circ$) for receiver function analysis (Figure 2). For a more detailed description of

the experiment and an analysis of its background noise characteristics, see *Wilson et al.* [2002].

3. Receiver Functions

3.1. Receiver Function Estimation

[6] Teleseismic body waves from earthquakes produce a series of reflections, refractions, and conversions as they traverse boundaries between regions of differing seismic velocity and/or impedance. Radial receiver function analysis emphasizes P -to- S converted arrivals at these interfaces via signal deconvolution between horizontal and vertical component seismograms [Langston, 1977; Ammon, 1991; Cassidy, 1992]. Commonly observed converted/refracted propagation modes in receiver functions include a pulse associated with the incoming P wave field, direct P -to- S (P_s) converted modes generated by the upcoming wave field at each discontinuity, and reverberated modes which are generated by the upcoming wave field being reflected downward off the earth's free surface as P or S , and finally reflecting upward as S at each discontinuity.

[7] To produce teleseismic images of P -to- S scattered energy caused by these seismic velocity and impedance contrasts, we applied receiver function estimation and filtering techniques described by *Wilson and Aster* [2005]. These techniques take advantage of characteristic moveout to enhance receiver function arrivals, while removing features attributable to noise and deconvolution instability. This is accomplished by first transforming receiver functions calculated at a single station from the time-slowness ($t - p$) domain to the frequency–pseudowave number ($f - \kappa$) domain using a two-dimensional Fourier transform. The pseudowave number κ has units of cycles/slowness, or cycles/(s/km). Receiver function amplitudes that have large variability as a function of p will map to high κ values in the $f - \kappa$ domain at a given frequency. This could occur due to either high-moveout arrivals (large dt/dp), or to receiver function features that do not appear on adjacent receiver functions and may, in fact, be caused by high background noise and/or instability in the receiver function deconvolution. By calculating the maximum predicted dt/dp we can calculate the maximum physically reasonable range of κ and design an $f - \kappa$ filter to attenuate receiver function amplitudes with high variability as a function of horizontal slowness while preserving arrivals with consistent moveout characteristics.

[8] Figure 3 illustrates the receiver function filtering process for a single station (NM24). Individual receiver functions were calculated using water level spectral division. The water level parameter was determined for each receiver function by performing the receiver function deconvolution for a range of water levels between 0.001 and 0.1 (between 0.1% and 10% of the maximum vertical seismogram spectral element). We then select the water level which has the lowest amount of energy arriving before time zero on the resulting receiver function. Figures 3a and 3b show unfiltered receiver function amplitudes in the $t - p$ (time-slowness) and $f - \kappa$ (frequency–pseudowave number) domains, respectively. A challenge in transforming receiver function amplitudes to the $f - \kappa$ domain is that earthquake arrivals at a given station are typically not regularly spaced as a function of p . To overcome this

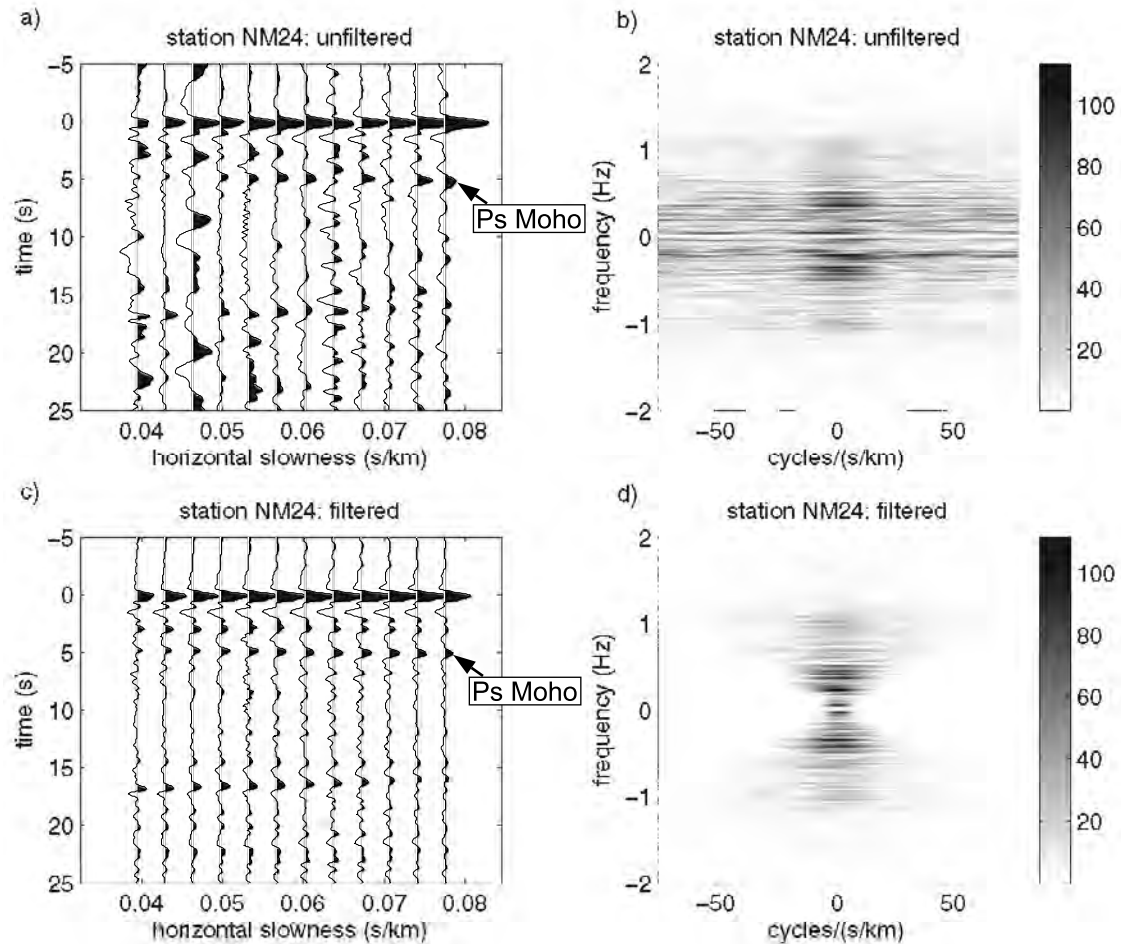


Figure 3. Receiver functions calculated for a single station (NM24) in the (a) $t - p$ domain and (b) $f - \kappa$ domain before filtering, and in the (c) $t - p$ domain and (d) $f - \kappa$ domain after filtering. Receiver functions have been binned into equally spaced p bins prior to transforming to the $f - \kappa$ domain.

problem we bin receiver functions into equally spaced bins of 0.0035 s/km resulting in a total of 12 bins for teleseisms from epicentral distances of 35–95°. We can then transform receiver function amplitudes to the $f - \kappa$ domain and apply the receiver function filtering technique described by *Wilson and Aster* [2005] in order to attenuate receiver function amplitudes that do not vary smoothly as a function of p , such as would be expected for uncorrelated noise effects. The resulting filtered receiver function arrivals are shown in Figures 3c and 3d in the $t - p$ and $f - \kappa$ domains, respectively. There is evident improvement in the $t - p$ domain, with a significant increase in the lateral coherency of receiver function arrivals.

3.2. Velocity Model Estimation

[9] By measuring the moveout of the direct converted and reverberated receiver function modes (assuming a local flat layered structure), it is possible to estimate local depth and average V_p/V_s ratio between the surface and the discontinuity associated with each mode [e.g., *Zandt and Ammon*, 1995]. In practice, individual modes can be difficult to observe and identify on individual traces, and stacking methodologies are commonly employed. By assuming a

starting average P wave velocity model, an estimate the local average crustal V_p/V_s ratio (ν) and thickness (H) at each station can be obtained by stacking receiver function amplitudes at the predicted direct converted phase (Ps) and reverberated phase ($PpPs$ and $PpSs + PsPs$) times for several receiver functions in the $H - \nu$ plane [*Zhu and Kanamori*, 2000]. The stacked trace amplitude will be maximized where the three modes add constructively, and measurement variances and covariances can be calculated from the solution peak. The main assumptions in this method are that the incoming P wave is essentially a plane wave, that the velocity structure is composed of locally flat layers, and that the crust is laterally uniform over the distances sampled by the direct and reverberating modes (20–50 km in this case). By using receiver functions from all azimuths and epicentral distances effects of lateral heterogeneity can be reduced to obtain an average crustal velocity and thickness estimate at each station.

[10] An important consideration in accurately estimating the crustal velocity model is an accurate characterization of the thickness and velocity of near-surface sediments. Because seismic velocities, particularly for shear waves, can be much slower for sedimentary rocks than for crystalline

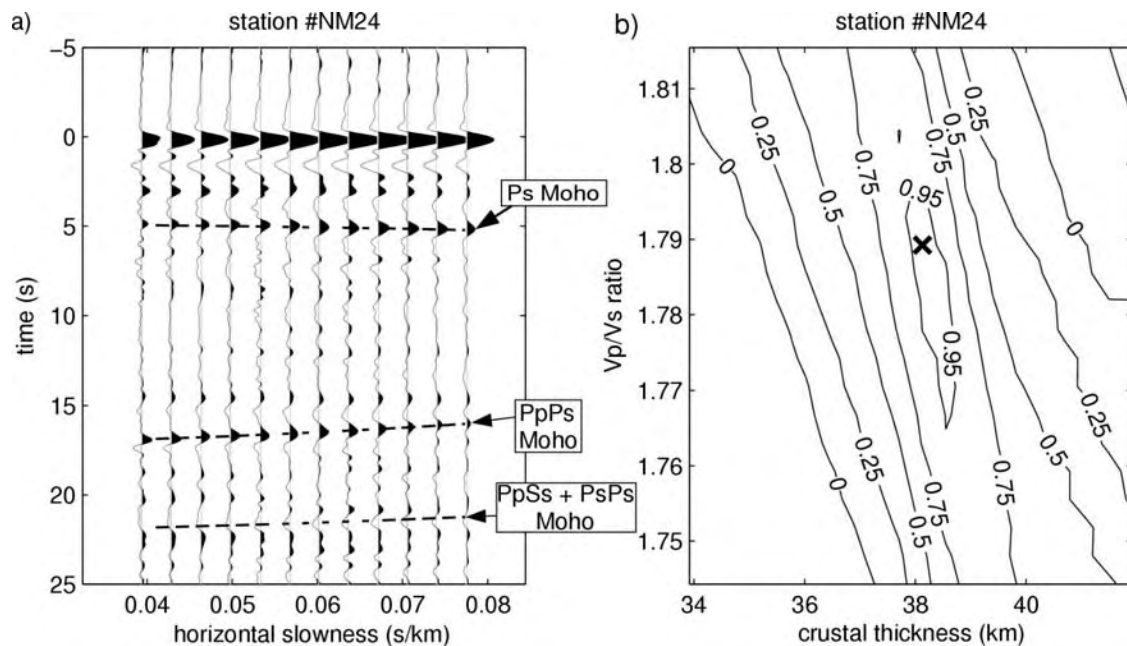


Figure 4. (a) Receiver functions calculated for a single station (NM24) using events at a range of epicentral distances. Direct converted phases have moveout curves that are opposite in sign to reverberated phases, allowing for the discrimination of arrival types. Dashed lines indicate best fit solutions obtained from moveout analysis. (b) Contour of amplitudes in the $H - \nu$ domain determined from moveout analysis. The best fit solution is indicated by the symbol X.

rocks, there is potential for shear wave ray paths to have travel times of several seconds within the deep sedimentary basins crossed by the RISTRA network, which is an appreciable fraction of the total travel time through the crust. Because of the strong impedance contrast between the rocks in the sedimentary basins and the crystalline Precambrian basement, sedimentary basins also produce large primary P_s and multiple modes. Before estimating crustal parameters, a variation of the *Zhu and Kanamori* [2000] method is thus applied to estimate the seismic velocities from the basin primary and multiple modes, where the layer thickness (H) is fixed, and a search is performed over a range of V_p and V_s to find the velocities for which the primary and multiple arrivals add constructively. Along RISTRA, the sedimentary layer thicknesses are well constrained in the Delaware and San Juan basins [e.g., *Sloss*, 1988] from extensive oil and gas exploration efforts. The predominantly Paleozoic sediments of the Delaware basin (TX01–NM10), which are up to 7 km thick, produce distinct primary and multiple modes, from which an average P wave velocity of 4.96 km/s and S wave velocity of 2.62 km/s ($V_p/V_s = 1.89$) has been estimated. The predominantly Mesozoic sediments of the San Juan basin (NM35–NM42), which are up to 2.2 km thick where the RISTRA network crosses, have sufficiently slow seismic velocities to also produce distinct primary and multiple modes, from which an average P wave velocity of 3.05 and S wave velocity of 1.35 ($V_p/V_s = 2.26$) has been estimated. However, this method of estimating the sedimentary layer velocities does not work well in areas of steeply dipping shallow structure. Examples are station TX01–TX02 (which are near the steep, fault-bounded edge of the Delaware basin's central basin platform), and NM28–

NM30 which are in the narrow Albuquerque-Belen basin (which is bounded by steeply dipping faults). In areas where it was impossible to determine sedimentary layer velocities, an intermediate velocity between those found for the Delaware basin and San Juan Basin was used, depending on the lithology of the local sedimentary layer.

[11] The starting crustal P wave velocity model used for velocity analysis was constructed using a host of published refraction results [e.g., *Roller*, 1965; *Stewart and Pakiser*, 1962; *Sinno and Keller*, 1986; *Topozada and Sanford*, 1976; *Olsen et al.*, 1979]. An example of receiver function moveout analysis is shown in Figure 4, and estimates of crustal thickness and V_p/V_s ratio along the RISTRA network are shown in Figure 5. Crustal thickness estimates range from 43 to 51 km in the Colorado Plateau and 39 to 50 km in the Great Plains. Crustal thickness estimates show a uniform and generally symmetrical thinning to approximately 35 km thick in the center of the RGR.

[12] Estimates of crustal average V_p/V_s ratios along the RISTRA array (Figure 5b) range from 1.71 to 1.80. This variability, as well as the associated error estimates, are in part due to the shape of the solution peak shown in Figure 4b, which is typically extended in the direction of the ν axis. However, a high level of variability, along with lateral variability in crustal thickness estimates, may indicate strong lateral velocity heterogeneity or considerable Moho topography. Since this method of velocity estimation assumes a locally flat, homogeneous velocity model, violating one or both of these assumptions will produce a potentially biased or uncertain result. The starting velocity model used for migration of receiver functions was constructed by averaging these results over a horizontal spatial scale of 90 km (5 stations), with V_p/V_s smoothly varying

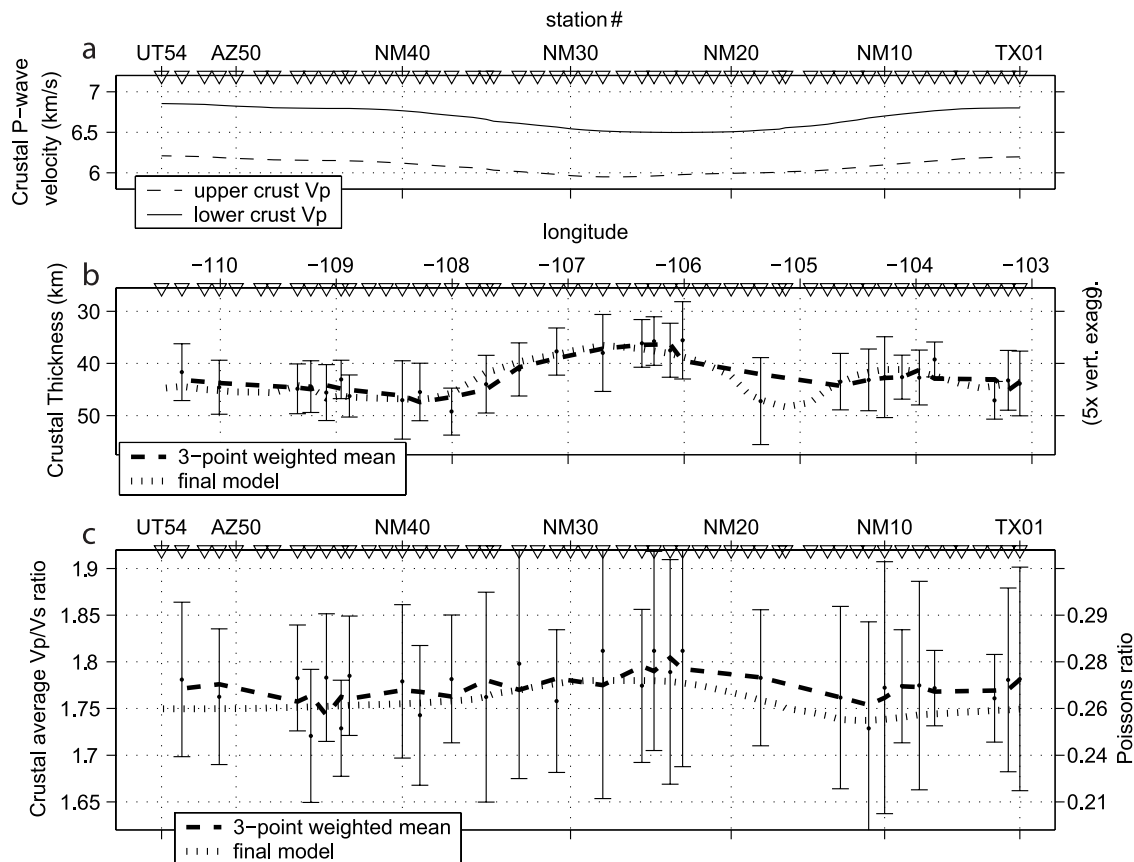


Figure 5. RISTRA crustal velocity model. (a) The starting crustal P wave velocity model used for velocity analysis constructed using a host of published refraction results [e.g., *Roller, 1965; Stewart and Pakiser, 1962; Sinno and Keller, 1986; Topozada and Sanford, 1976; Olsen et al., 1979*]. (b) Estimates of crustal thickness and (c) V_p/V_s ratio from receiver function moveout analysis.

from 1.74 in the Great Plains, to 1.78 near the RGR, to 1.75 in the Colorado Plateau.

3.3. Receiver Function Migration

[13] Receiver functions were first applied to solitary stations to obtain local one-dimensional structure estimates [e.g., *Langston, 1977*]. As the number of stations available for deep seismic imaging has increased, receiver function techniques have been extended to create (to date, frequently two-dimensional) images of fundamental structures such as the Moho or upper mantle transition zone discontinuities [e.g., *Sheehan et al., 1995; Yuan et al., 1997; Li et al., 2002*]. Here we apply receiver function migration methodology developed by *Wilson and Aster [2005]* that uses information contained in both direct and reverberated P -to- S converted energy while suppressing reverberation artifacts.

[14] The RISTRA experiment recorded multicomponent broadband seismic data along a notably long (approximately 950 km), densely occupied (approximately 18 km interstation spacing), and uniform (interstation spacing standard deviation of 3.6 km) transect that is especially well suited for applying seismic migration techniques. We first apply a regularized Kirchhoff receiver function migration method [*Wilson and Aster, 2005*] for prominent P -to- S converted modes to produce corresponding lithosphere-scale seismic scattering potential images. Figure 6a shows the P_s mode-migrated receiver function cross section. First-order

features visible in Figure 6a include the direct conversion from the bottom of the Delaware basin (stations TX01–NM10) at 5–7 km depth, as well as strong basin multiple modes, which, because of their differing ray geometry, are migrated to an incorrect depth range of 20–30 km to reside directly beneath the correctly imaged P_s mode. The P_s mode generated at the Moho is also evident, occurring prominently at 35–50 km depth across the entire transect. This image also shows apparent subcrustal discontinuities. However, in a single mode cross section, such as Figure 6a, it is difficult to discern if such apparent discontinuities are actually due to P_s energy migrated to the correct depth, or whether they are imaging artifacts arising from multiple modes generated from shallower features and improperly migrated. For the P_s migration a bandpass filter (second-order Butterworth filter) between 1.5 and 15 s was used.

[15] The migrated image of the $PpPs$ mode is shown in Figure 6b, in which the $PpPs$ phase generated at the Moho (which was incorrectly imaged at 150–170 km depth in the P_s migration of Figure 6a), has now been moved to the correct depth range of 35–50 km. However, Figure 6b contains imaging artifacts, for example, associated with P_s mode energy, which is now incorrectly migrated to shallower depth. This can clearly be seen for the Moho P_s phase, which is mapped to near 10 km in Figure 6b. Similarly, the migrated image of the $PpSs + PsPs$ phase

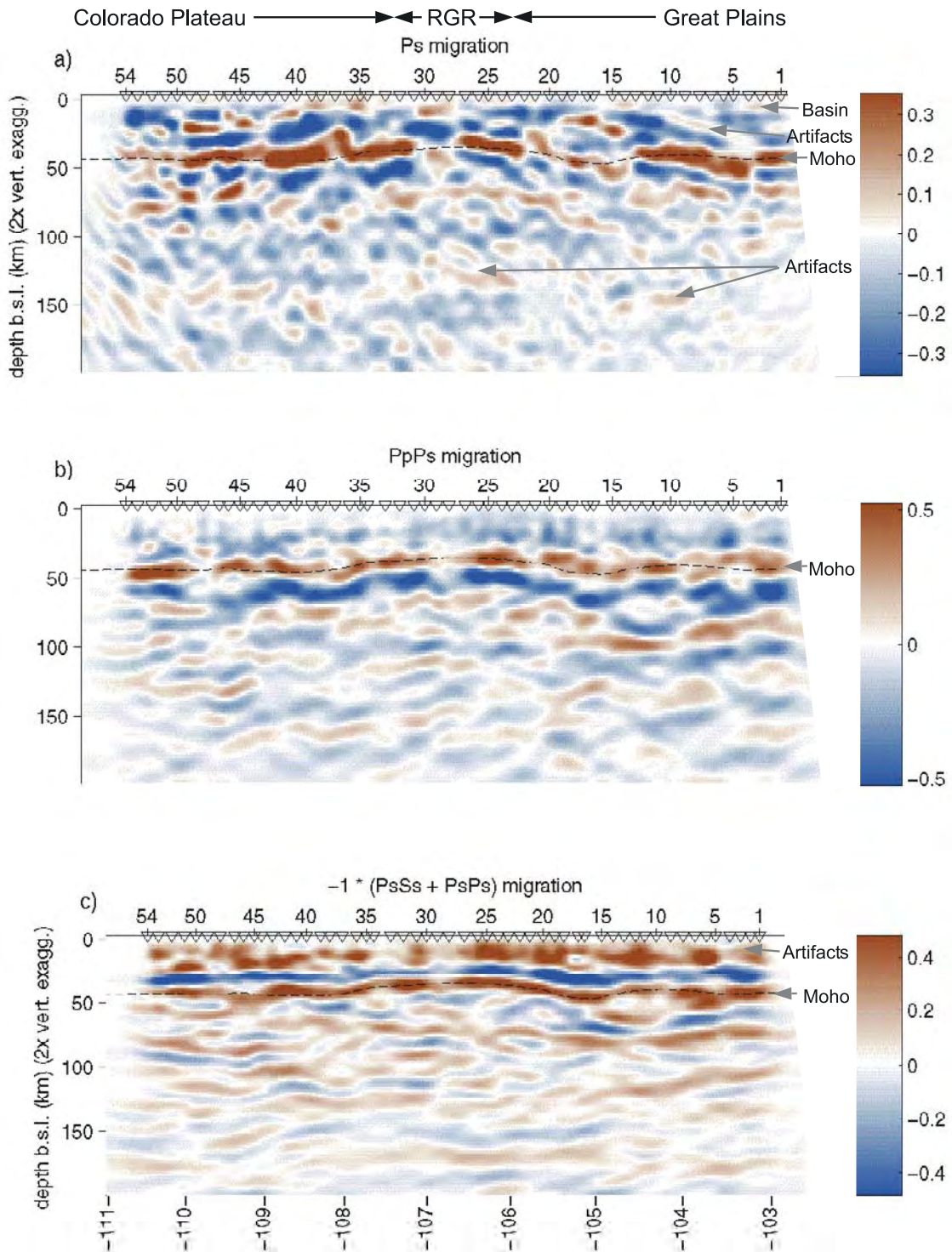


Figure 6. Migrated cross sections for the (a) *Ps*, (b) *PpPs*, and (c) *PpSs + PsPs* phases. Positive amplitudes indicate a negative seismic impedance change moving upward. Each single mode migration shows a prominent Moho signal but may include significant artifacts associated with the improper migration of energy arriving from other modes.

(Figure 6c), has the seismic energy for this mode placed at the correct depth, but has its own imaging artifacts associated with the *Ps* and *PpPs* modes which are each mapped more shallowly than their correct depth. For the *PpPs* and *PpSs + PsPs* migrations a bandpass filter (second-order Butterworth filter) between 6 and 30 seconds s was used. The relatively

good depth alignment of the Moho in the *Ps*, *PpPs*, and *PpSs + PsPs* migrations (Figure 6) confirms the accuracy of the velocity model used for migration [Wilson and Aster, 2005].

[16] Forward modeled resolution [Wilson and Aster, 2005] for the lithosphere-scale migration of Figure 6 is shown in Figure 7. This analysis is analogous to resolution

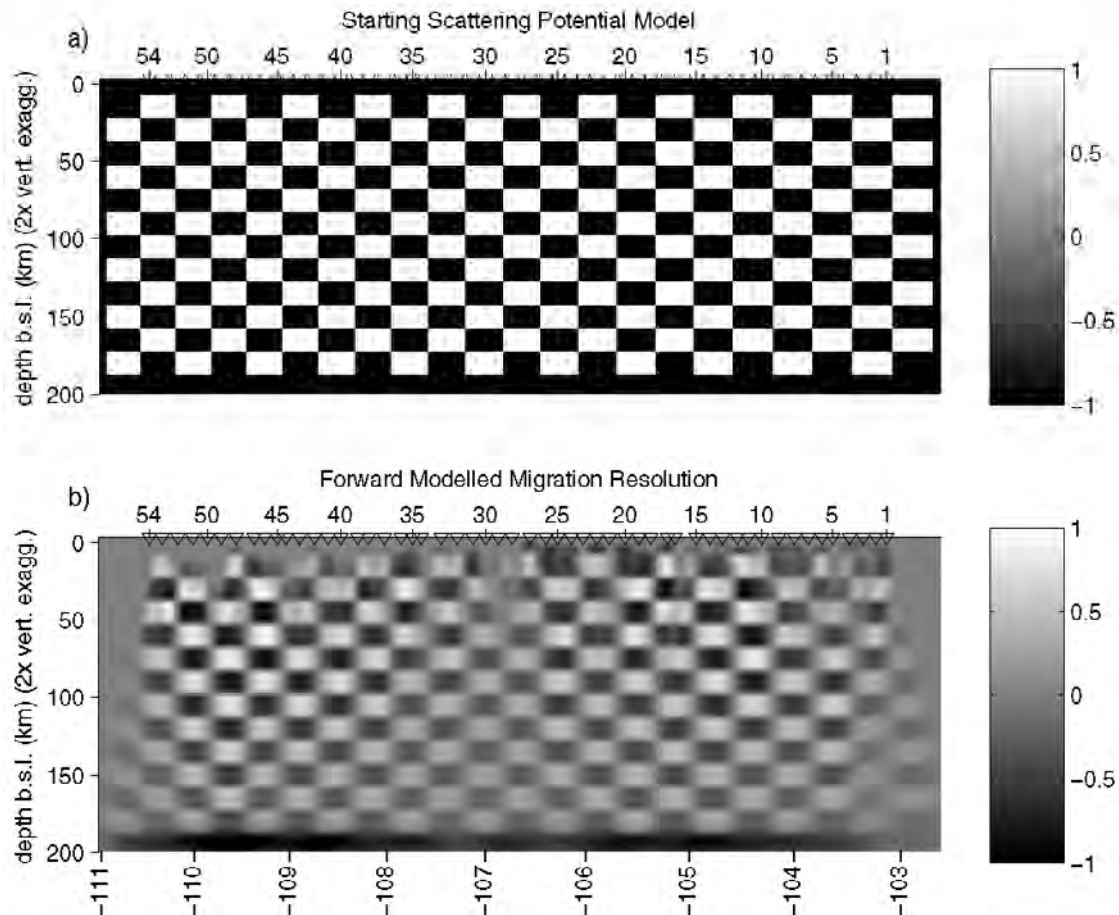


Figure 7. Forward modeled resolution of the lithosphere-scale migration [Wilson and Aster, 2005].

tests commonly performed in tomographic inversions, and assesses bias introduced by regularization and/or rank deficiency into the linear inverse problem for a general Earth structure (which is a solely function of station spacing and data coverage). Regularized migration does an excellent job recovering the starting model, with minimal evident lateral variation in receiver function amplitudes. This indicates that the number of receiver functions used in the imaging, and their associated ray paths, provide ample coverage of the imaged region. Migration resolution decays rapidly off the ends of the network, but does extend slightly further off the northwestern edge of the network due to a larger number of receiver functions used from the northwest.

[17] A lithosphere-scale, nonlinearly stacked, multiple mode image [Wilson and Aster, 2005] is shown in Figure 8. The technique stacks migrated grids from multiple modes to cancel imaging artifacts arising from mismigrated energy (Figure 6), and to consequently enhance features that map to the same depths. This is accomplished by a nonlinear stacking technique [Wilson and Aster, 2005] that produces large amplitudes in the final image only when the P_s , $PpPs$, and the negative (due to reflection polarity reversal) of the $PpSs + PsPs$ migration images have identical polarity. The most prominent horizon in the stacked image is the Moho, which appears 40–50 km beneath the Colorado Plateau and Great Plains, and thins to a minimum of 35 km at the center of the Rio Grande Rift. A number of intriguing subcrustal

discontinuities can also be seen, the most prominent of which is a northwestern dipping ($\sim 6.4^\circ$) feature 65–85 km depth beneath the Colorado Plateau. Discontinuities can also be seen 70–85 km beneath the center of the Rio Grande Rift and 50–120 km beneath the Great Plains. The multimode stacking technique greatly enhances consistent features from the three migrations while attenuating incorrectly migrated energy. However, some artifacts still appear in Figure 8. Sporadic seismic energy is present at ~ 150 km depth along the network, which is the depth that the very strong crustal multiples appear in the P_s migrated cross section (Figure 6a). Other imaging artifacts occur at ~ 10 km depth beneath stations NM09–NM12 and NM38–NM42. These are attributable to imaging artifacts from the P_s phase image (from the strong $PpPs$ and $PpSs + PsPs$ multiples generated in the low-velocity sediments of the San Juan and Delaware Basins) coincidentally aligning with imaging artifacts in the reverberated phase images (from the Moho P_s energy which is incorrectly imaged at lesser depth). Thus, although the stacked receiver function image provides a valuable tool in assessing the alignment of receiver function phases, the persistence of some artifacts shows that interpretation should be done using both the individual phase migrations and the stacked cross section.

[18] Figure 9 shows an upper mantle transition zone-scale receiver function image using the migrated P_s phase only. We found, for the RISTRA data set, that reverberated

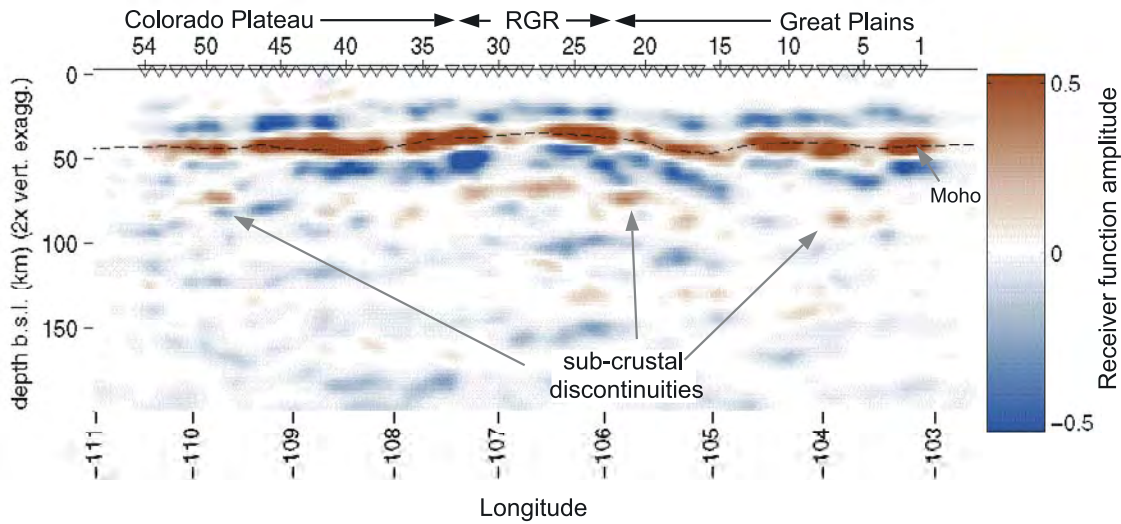


Figure 8. Nonlinear stack [Wilson and Aster, 2005] of the migrated lithosphere-scale cross sections of Figure 6.

receiver function modes originating from structures at depths greater than 200 km were not useful for the type of multimode analysis used in the lithosphere-scale images of Figure 6. We suspect that this occurs because they lack coherence and are attenuated due to long delay times (greater than 100 s) relative to the first *P* wave arrival, and because they traverse a much larger lateral distances and are therefore much more strongly influenced by lateral velocity, and possibly topographic, heterogeneity. Figure 9 shows that the 410 and 660 km mantle discontinuities are relatively flat, showing variations less than 20 km across the entire transect. A prominent feature is also observed at approximately 250 km depth, showing highest amplitude beneath the northwestern half of the network, and appearing

to deepen to the southeast after traversing the RGR. The forward modeled upper mantle migration resolution analysis is shown in Figure 10, and shows good lateral continuity of receiver function amplitudes. The resolution degradation caused by having fewer events from South America in the RISTRA data set than from source zones to the northwest is more apparent in the deep migration resolution than in the shallower migration of Figure 7.

4. Discussion

4.1. Colorado Plateau

[19] The average crustal thickness of the Colorado Plateau along the RISTRA transect (45.6 ± 1.1 km) is only

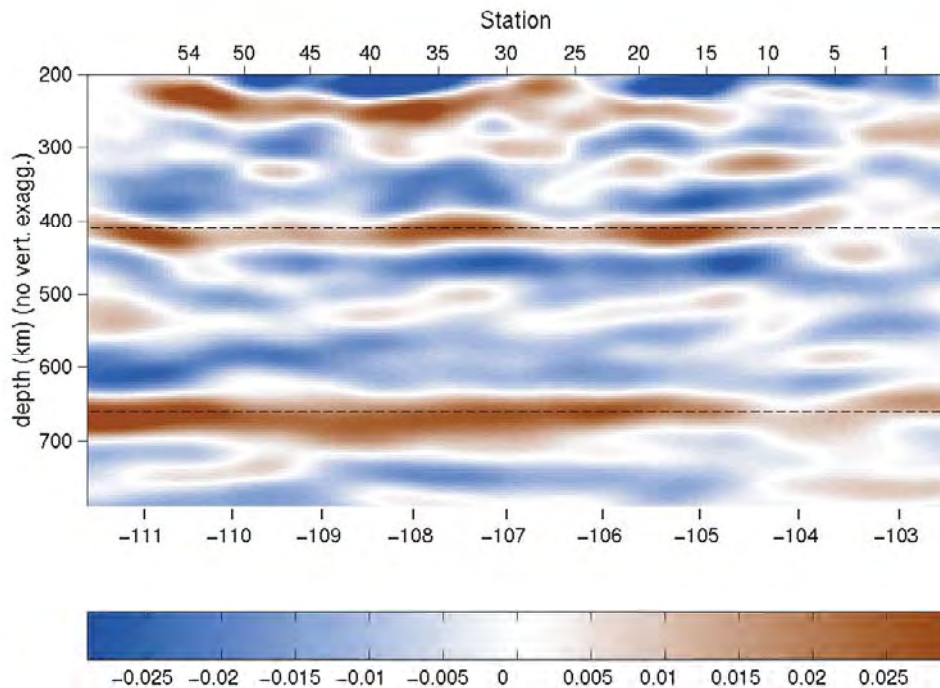


Figure 9. Migrated *Ps* mode receiver function image of the upper mantle.

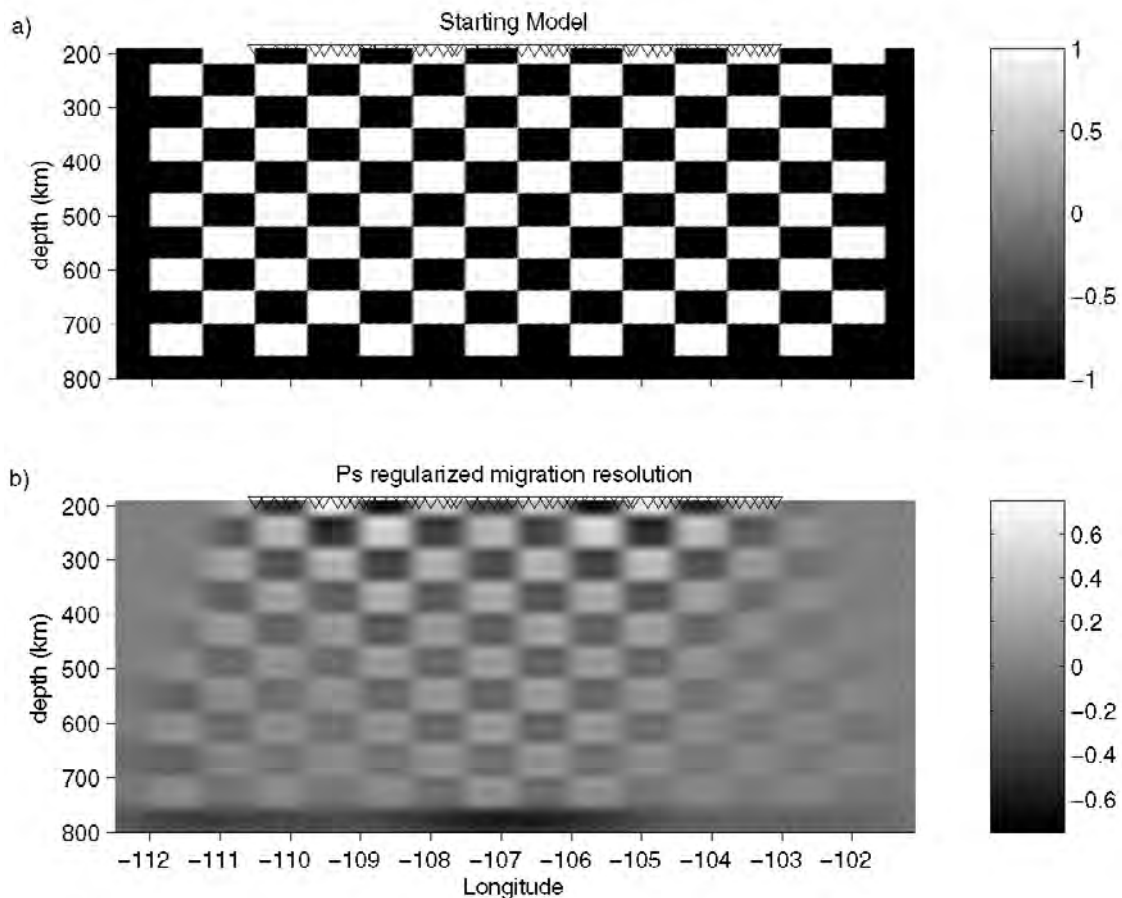


Figure 10. Forward modeled resolution for the upper mantle migration.

modestly thicker than that of the Great Plains (44.1 ± 2.3 km; Figure 8). However, the Colorado Plateau has an elevation (~ 2 km above sea level) that is approximately 1 km higher than that of the great plains. The amount of isostatic buoyancy provided by an additional crustal thickness of 1.5 km would result in approximately 0.3 km of additional elevation (assuming and crust and mantle densities of 2.7 and 3.3 g/cm^3 , respectively). This suggests that the high elevation of the plateau is not entirely due to shallow compensation by typical thickened crust above normal mantle. Thus the Colorado Plateau either features a more buoyant crustal and/or mantle density contrast, or is supported dynamically. Analyses of crust and mantle xenoliths from the Navajo volcanic field, located in the heart of the Colorado Plateau, have provided insight to the composition, age, and tectonic history of Colorado Plateau crust and mantle. Xenoliths from multiple crustal levels show mid-Proterozoic ages (1.7–2.0 Ga) with no indication of later magmatic underplating [Wendlandt *et al.*, 1993]. Because the Colorado Plateau has experienced relatively minor deformation compared to its surrounding tectonic provinces, this suggests that structures associated with crustal formation and accretion may still be preserved. Selverstone *et al.* [1999] suggest that compositional changes in crustal xenoliths across the Navajo field are consistent with a northwest dipping Proterozoic subduction zone, with the crustal suture located near where RISTRA crosses the Arizona/New Mexico border (station NM44; Figure 11). We

note that this location corresponds with the eastern extent of a northwestern dipping ($\sim 6.4^\circ$) discontinuity at 65–85 km depth beneath the Colorado Plateau (Figures 8 and 11), as well as coincident with the western edge of the San Juan basin, expressed at the Hogback monocline.

[20] Recent surface wave inversion results from the RISTRA network [West *et al.*, 2004] show a high-velocity lithospheric root beneath the Colorado Plateau to 140–160 km depth. Mantle xenolith data from the Colorado Plateau suggest that the subcrustal lithosphere is relatively depleted in Fe rich olivine [Smith, 2000; Lee *et al.*, 2001] which could increase the buoyancy of the Colorado Plateau. Mantle xenolith data further suggests that at the time of eruption (30–20 Ma), the Colorado Plateau was characterized by a cool root analogous to those beneath Archean cratons, with compositional similarity to oceanic lithosphere [Roden and Shimizu, 1993, 2000]. This cool root may extend to depths up to 140 km [Riter and Smith, 1996] and has mid-Proterozoic U-Pb zircon ages [Smith *et al.*, 2002]. If the subcrustal lithosphere beneath the Colorado Plateau is mid-Proterozoic and has a compositional similarity to oceanic lithosphere, then the subcrustal discontinuities imaged in the receiver function cross sections could represent subducted slabs which have been trapped in the lithosphere since Proterozoic terrane accretion. Proterozoic suture zones within the crust are typically proposed to be more steeply dipping [e.g., Selverstone *et al.*, 1999] than the northwestern dipping ($\sim 6.4^\circ$) discontinuity observed at 65–

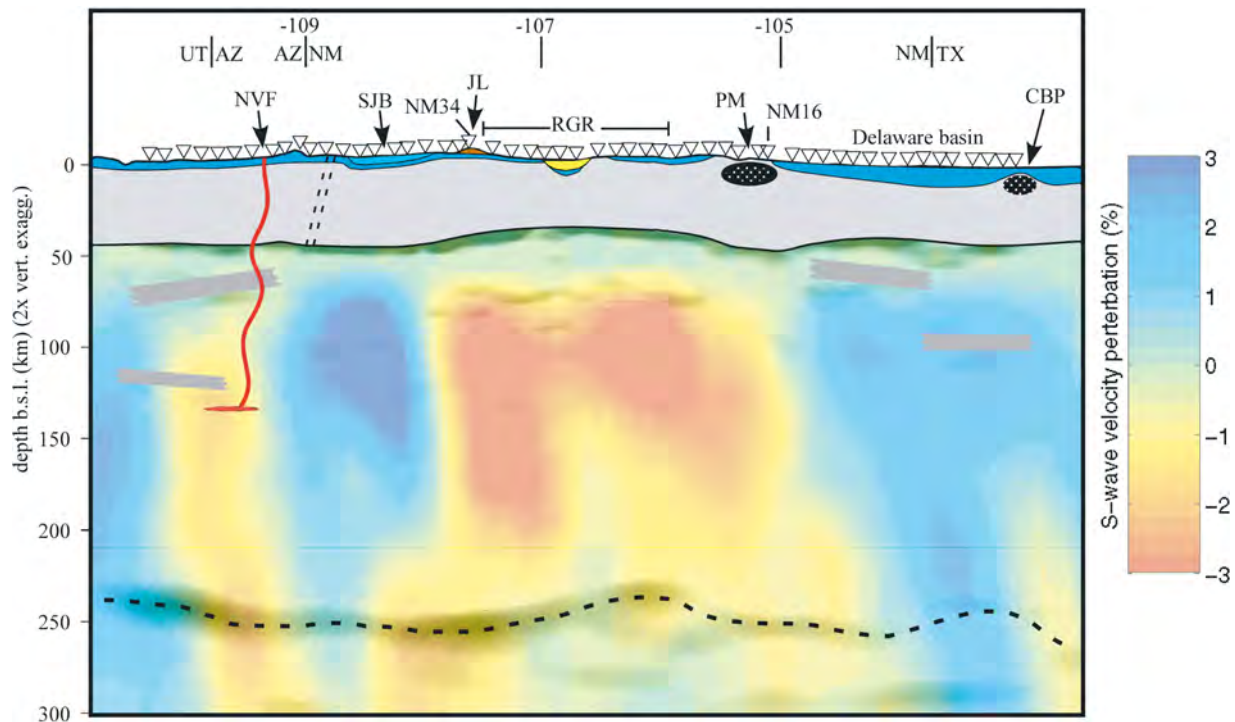


Figure 11. Schematic diagram showing the relationship between LA RISTRA lithospheric interpretations and surface geologic features including the Navajo volcanic field (NVF), the San Juan basin (SJB), the Jemez lineament (JL) expressed at Mount Taylor, the Rio Grand rift (RGR), Pajarito Mountain (PM), the Delaware basin, and the central basin platform (CBP). Upper mantle color scale indicates relative velocity structure as determined from body wave tomography [Gao *et al.*, 2004]. Positive receiver function amplitudes are overlain in gray scale. The upper 10 km has been exaggerated 10 times to show topography and basin depth. The double dashed line indicates the proposed location of a northwest dipping Proterozoic suture zone from Selverstone *et al.* [1999].

85 km depth beneath the Colorado Plateau (Figure 8). We propose that this subcrustal structure may represent Proterozoic oceanic crust that was subducting to the northwest at a relatively shallow angle because it was relatively young and therefore had elevated temperatures [Selverstone *et al.*, 1999]. A thick and cool lithospheric root would not contribute to the buoyancy of the Colorado Plateau. However, surface wave inversion results by West *et al.* [2004] have identified an asthenospheric low-velocity channel between 150 and 300 km depth, and demonstrate that it is adequate to provide the added buoyancy to support approximately 1.3 km of the high elevation of the Colorado Plateau. This added buoyancy, along with the added buoyancy from slightly thickened crust, explains the elevation of the Colorado Plateau.

4.2. Rio Grande Rift

[21] Extensional deformation of the lithosphere can be characterized by two end-member models, characterized by either pure shear [e.g., McKenzie, 1978] or simple shear [e.g., Wernicke, 1985]. The pure shear model is characterized by a brittlely deforming upper crustal layer and a ductilely deforming lower crust and mantle lithosphere. This produces symmetric thinning and a symmetric lithospheric cross section with the region of greatest lithospheric and crustal thinning located directly beneath the rift axis. The simple shear model is characterized by shear along a low-angle master detachment fault which may conceivably

span the entire lithosphere. This produces an asymmetric lithospheric cross section with the region of greatest crustal thinning offset laterally from the region of greatest mantle lithosphere thinning. This offset can, in turn, produce asymmetry in heat flow, flexural uplift, and thermal uplift [Buck *et al.*, 1988].

[22] Geochemical analysis of volcanic rocks from the RGR indicates a temporal transition from rocks with a lithospheric source to rocks with an asthenospheric source [Perry *et al.*, 1988], which is interpreted as a thinning of the lithosphere. Further analysis indicates that the lithosphere has thinned relatively symmetrically and that the greatest lithospheric thinning is centered beneath the axis of the rift [Baldridge *et al.*, 1991; McMillan, 1998], favoring a pure shear mode of deformation. Analysis of gravity data also indicates a symmetric thinning of the lithosphere which closely tracks the rift axis [Cordell *et al.*, 1991]. Surface wave inversions [West *et al.*, 2004] and tomography results [Gao *et al.*, 2004] (Figure 11) from RISTRA data show a zone of low velocity ranging from 65 to 125 km depth, centered beneath the rift. These lines of evidence, along with the symmetric thinning of the crust observed in receiver function images (Figures 8 and 11) indicate an overall pure shear extensional mechanism for the Rio Grande Rift lithosphere.

[23] Upper mantle receiver function results (Figure 9) show negligible topography on the 410 km (exothermic, α -olivine to β -spinel) and 670 km depth (endothermic; γ -spinel to perovskite) mantle discontinuities, which indicates

a lack of a localized thermal anomaly under the region at these depths. However, other mineral transitions such as majorite-perovskite which also occurs around 670 km depth, and has a positive pressure-temperature slope, may decrease the magnitude of the depth change predicted for the 670 km discontinuity [Akaogi and Ito, 1999]. A strong increase in temperature associated with a deep mantle upwelling would be expected to compress the transition zone thickness by around 15 km per 100°C [Bina and Helffrich, 1994]. However, because the overall transition zone thickness does not change significantly, the observed flat structure suggests that mantle temperatures 410 to 670 km beneath the RGR do not have a strong lateral variation, and that the thermal signature of the RGR is predominantly confined to the uppermost mantle at less than 400 km depth.

[24] An apparent Lehmann discontinuity [Lehmann, 1959] observed at ~250 km depth (Figure 9) shows highest amplitude beneath the northwestern half of the network, and appears to deepen and lose continuity to the southeast. A similar discontinuity was reported in the eastern United States beneath the MOMA (Missouri to Massachusetts) PASSCAL experiment by Li *et al.* [2002]. The MOMA discontinuity appears at 270–280 km depth at the easternmost extent of MOMA, and gradually deepens and becomes more complex in its western third. This discontinuity is not observed globally in long-period stacks [Shearer, 1991], either because its depth is highly variable and/or it is not sufficiently widespread. Analysis of SS precursors [Gu *et al.*, 2001] indicates that the Lehmann discontinuity is present beneath 50% of continental regions and only 25% of oceanic regions.

[25] The origin of the discontinuity is debatable, one possibility being that it is associated with the base of an asthenospheric low-velocity zone [Leven, 1981; Li *et al.*, 2002]. The discontinuity could also represent a phase change in clinoenstatite pyroxenes which lattice dynamic modeling indicates could cause a change in *P* wave velocity of 6.18% [Mendelsohn and Price, 1997]. Another possibility is that the discontinuity represents a shear-induced anisotropic boundary [Revenaugh and Jordan, 1991; Karato, 1992] representing the transition in deformation mechanism from diffusion creep below to dislocation creep above the discontinuity. A test of this hypothesis for RISTRA was performed by examining receiver function conversion amplitudes as a function of back azimuth and no significant azimuthal variability was noted. However, this is possibly due to inadequate azimuthal coverage given that analysis of RISTRA SKS data [Gök *et al.*, 2003] shows high levels of anisotropy that correlate with low velocities beneath the RGR and Colorado Plateau. If the ~250 km depth discontinuity is linked to the base of an upper mantle low-velocity zone, it may represent the base of the asthenospheric low-velocity channel identified by West *et al.* [2004]. This is also supported by the observation that this discontinuity loses receiver function amplitude in the southeastern third of the network (Figure 9) which corresponds to the southeastern truncation of the West *et al.* low-velocity channel. We also note that the observed small-scale variations in the apparent depth to the Lehmann discontinuity correspond with small-scale velocity changes (Figure 11), with the discontinuity generally appearing deeper in regions of low velocity. However, for all the possible origins of the

Lehmann discontinuity listed above, depth variations would be expected due to changes in composition, stress, and/or thermal conditions.

4.3. The Great Plains

[26] In the individual mode migrated cross sections (Figure 6), strong reverberations from the Delaware basin are evident that interfere with Moho and deeper direct conversion structural information. However, as the other migrated images are stacked, these reverberations become greatly attenuated, thus showing that the stacking technique of Wilson and Aster [2005] can usefully suppress even strong basin multiples in receiver function migration applications. Great Plains crustal thickness ranges from 41–48 km, averaging 44.1 ± 2.3 km (Figure 8). An apparent crustal thickening, centered near NM16, is located near Pajarito Mountain (Figure 11, a Precambrian exposure that has been a topographic high for the majority of the Phanerozoic [Bowsher, 1991]). Gravity and magnetic data indicate Pajarito Mountain is underlain by a large, dense, ultramafic intrusion which may have been emplaced during late Proterozoic rifting [Bowsher, 1991; Roberts *et al.*, 1991]. This intrusive body is near the southern edge of the Pedernal uplift (Figure 1) which underwent extensive uplift during the late Paleozoic and Laramide. Much of the region crossed by the southeastern portion of RISTRA (TX01–NM10) may have been extending in a back arc basin setting while arcs were accreting to the continent further southeast (1290–1230 Ma). Later continental rifting, and associated mafic intrusions into the upper crust, may have occurred (1150–1120 Ma) in the location of present-day faults associated with the central basin platform (TX01–TX02; Figures 1 and 11 [Mosher, 1998; Kluth and Coney, 1981]), and much of the structural development of the Delaware basin was controlled by these preexisting structures [Keller *et al.*, 1980]. Crustal thickening observed in receiver function images near station NM16 and TX01–TX02 (Figure 8) may be an expression of these structures which have had a major influence on regional tectonics.

[27] This region of crustal thickening also coincides with the location of a prominent high-velocity lithosphere-scale feature visible in surface wave and body wave tomography (Figure 11) that may represent delaminating lithosphere [Gao *et al.*, 2004; West *et al.*, 2004] in a process comparable to the “mantle drip” under the Sierra Nevada [Benz *et al.*, 1992; Zandt, 2003]. We observe several dipping subcrustal discontinuities beneath the Great Plains, but unlike the Colorado Plateau (see above), the region lacks extensive xenolith data to provide insight into lithospheric composition and age. However, exposures across the Grenville front, document more than 300 m.y. of orogenic activity, including arc-continent and continent-continent collision [e.g., Mosher, 1998]. While the Grenville collisional suture is expressed at the surface near the southeasternmost extent of RISTRA in western Texas, associated subducted oceanic crust could be emplaced well beneath stations to the northwest.

5. Conclusions

[28] A detailed seismic cross section of crust and upper mantle structures along an approximately 1000-km-long

transect of the U.S. southwest is presented. The images were constructed using data from the Colorado Plateau/Rio Grande Rift Seismic Transect (RISTRA) experiment, a dense deployment of broadband seismometers spanning the Great Plains, Rio Grande Rift (RGR), and approximately 50% of the Colorado Plateau [Wilson *et al.*, 2002, 2003]. Receiver function-based *P*-to-*S* forward scattering imaging of seismic impedance contrasts was performed by applying migration and nonlinear stacking of multiple receiver function modes [Wilson and Aster, 2005]. The migrated Moho image shows dramatic (~10 km or 22%) rift-symmetric crustal thinning beneath the RGR, and indicates significant short-wavelength topography and impedance contrast variability (e.g., thickness changes of up to 7 km over lateral distances of less than 100 km). The thinnest crust is centered along the RGR axis, suggesting a pure shear thinning mechanism for the Cenozoic rift-associated thinning of the lithosphere, a deformational model that is further supported by a rift-centered region of low velocities observed in surface wave inversions and tomography [West *et al.*, 2004; Gao *et al.*, 2004], as well as by regional isotopic data. Interestingly, crustal thickness estimate standard deviations from the RGR Moho upwarp region are somewhat tighter, and suggest a relatively smooth Moho that may have been altered by extension and/or thermal alteration, while those from the Colorado Plateau and Great Plains show much more lateral variability (Figure 5). Colorado Plateau crust is an average of 1.5 km thicker than Great Plains crust, and accounts for up to 0.3 km of Colorado Plateau elevation. This crustal thickening, coupled with buoyancy added by a deep, low-velocity channel imaged in surface wave analysis [West *et al.*, 2004], may explain the high elevation of the Colorado Plateau. We observe a prominent northwest dipping discontinuity 65–85 km beneath the Colorado Plateau, as well as additional possible subcrustal discontinuities beneath the Great Plains. These features, along with recent xenolith data, in the case of the Colorado Plateau, may indicate preserved Proterozoic lithospheric structures such as subducted oceanic crust associated with continental accretion. We observe a spatially variable upper mantle discontinuity at 250–300 km depth that may correlate with similar Lehmann discontinuities observed beneath eastern North America and elsewhere. The discontinuity is inconsistent with an anisotropic discontinuity but may represent the base of an asthenospheric low-velocity channel inferred from surface wave dispersion [West *et al.*, 2004]. We also observe relatively flat discontinuities at 410 and 660 km, indicating the lack of a strong thermal anomaly beneath the RGR at these depths, and that RGR processes are confined to the shallow mantle.

[29] **Acknowledgments.** RISTRA could not have occurred without the permission and other assistance of dozens of private landowners, the New Mexico State Land Office, the U.S. Forest Service, the U.S. Bureau of Land Management, the U.S. Fish and Wildlife Service, the Southern Utah Wilderness Alliance, Isleta Pueblo, Laguna Pueblo, Diné College, and the Navajo Nation. Persons wishing to conduct geological investigations on the Navajo Nation must first apply for and receive a permit from the Navajo Nation Minerals Department, P.O. Box 1910, Window Rock, AZ 86515, 928-871-6587. This study was supported by NSF grants EAR 9707190, EAR 9706094, and EAR 0207812. We also thank Los Alamos National Laboratory IGPP and the NMSU Arts and Sciences Research Center for support. The RISTRA team especially thanks the IRIS PASSCAL Instrument Center at New Mexico Tech and the IRIS Data Management System for essential equipment, planning, and data

archival assistance. RISTRA data are archived at and available from the IRIS Data Management Center (<http://www.iris.edu>) using network code XM for years 1999–2001. Essential field contributions were provided by Joe Leon, Eric Matzel, Richard Rapine, Frederik Tilmann, Wei-Chuang Huang, Al Blackhorse, Anca Rosca, Laurencita Luna, and Ducker's Diggers.

References

- Akaogi, M., and E. Ito (1999), Calorimetric study on majorite-perovskite transition in the system $Mg_4Si_4O_{12}$ - $Mg_3Al_2Si_3O_{12}$: Transition boundaries with positive pressure-temperature slopes, *Phys. Earth Planet. Inter.*, *114*, 129–140.
- Ammon, C. J. (1991), The isolation of receiver effects from teleseismic *P*-wave-forms, *Bull. Seismol. Soc. Am.*, *81*, 2504–2510.
- Baldrige, W. S., F. V. Perry, D. T. Vaniman, L. D. Nealey, B. D. Leavy, A. W. Laughlin, P. Kyle, Y. Bartov, G. Steinitz, and E. S. Gladney (1991), Middle to late Cenozoic magmatism of the southeastern Colorado Plateau and central Rio Grand rift (New Mexico and Arizona, U.S.A.): A model for continental rifting, *Tectonophysics*, *197*, 327–354.
- Benz, H. M., G. Zandt, and D. H. Oppenheimer (1992), Lithospheric structure of northern California from teleseismic images of the upper mantle, *J. Geophys. Res.*, *97*, 4791–4807.
- Bina, C., and G. Helffrich (1994), Phase transition Clapeyron slopes and transition zone seismic discontinuity topography, *J. Geophys. Res.*, *99*, 15,853–15,860.
- Bowring, S. A., and K. E. Karlstrom (1990), Growth, stabilization, and reactivation of Proterozoic lithosphere in the southwestern United States, *Geology*, *18*, n. 12, 1203–1206.
- Bowsher, A. (1991), Some effects of Precambrian basement on the development of the Sacramento Mountains, *Field Conf. Guideb. N. M. Geol. Soc.*, *42*, 81–89.
- Buck, R. W., F. Martinez, M. S. Steckler, and J. R. Cochran (1988), Thermal consequences of lithospheric extension: Pure and simple, *Tectonics*, *7*, 213–234.
- Cassidy, J. F. (1992), Numerical experiments in broadband receiver function analysis, *Bull. Seismol. Soc. Am.*, *82*, 1453–1474.
- Condie, K. C. (1982), Plate-tectonics model for Proterozoic continental accretion in the southwestern United States, *Geology*, *10*, 37–42.
- Condie, K. C. (1986), Geochemistry and tectonic setting of Early Proterozoic supracrustal rocks in the southwestern United States, *J. Geol.*, *94*, 845–864.
- Condie, K. C., and J. Selverstone (1999), The crust of the Colorado Plateau: New views of an old arc, *Geology*, *107*, 387–397.
- Cordell, L., Y. A. Zorin, and G. R. Keller (1991), The decompensative gravity anomaly and seep structure of the region of the Rio Grande Rift, *J. Geophys. Res.*, *96*, 6557–6568.
- Dickinson, W. R., and W. S. Snyder (1978), Plate tectonics of the Laramide Orogeny, *Mem. Geol. Soc. Am.*, *151*, 355–366.
- Frey, B. A., K. C. Condie, and R. Kerrich (2001), The Iron King Volcanics: A remnant of an oceanic plateau accreted to southwestern Laurentia 1.7 Ga, *Geol. Soc. Am. Abstr. Programs*, *33*(5), 24.
- Gao, W., S. Grand, W. S. Baldrige, D. Wilson, M. West, J. Ni, and R. Aster (2004), Upper mantle convection beneath the central Rio Grande Rift imaged by *P* and *S* wave tomography, *J. Geophys. Res.*, *109*, B03305, doi:10.1029/2003JB002743.
- Gök, R., et al. (2003), Shear wave splitting and mantle flow beneath LA RISTRA, *Geophys. Res. Lett.*, *30*(12), 1614, doi:10.1029/2002GL016616.
- Gu, Y. J., A. M. Dziewonski, and G. Ekstrom (2001), Preferential detection of the Lehmann discontinuity beneath continents, *Geoph. Res. Lett.*, *28*, 4655–4658.
- Humphreys, E. D. (1995), Post-Laramide removal of the Farallon slab, western United States, *Geology*, *23*, 987–990.
- Karato, S. (1992), On the Lehmann discontinuity, *Geophys. Res. Lett.*, *19*, 2255–2258.
- Keller, G. R., J. M. Hills, and R. Djeddi (1980), A regional geological and geophysical study of the Delaware basin, New Mexico and east Texas, *Field Trip Guideb. N. M. Geol. Soc.*, *31*, 105–111.
- Kluth, C. F., and P. J. Coney (1981), Plate tectonics of the ancestral Rocky Mountains, *Geology*, *9*, 10–15.
- Langston, C. A. (1977), Corvallis, Oregon, crustal and upper mantle receiver structure from teleseismic *P* and *S* waves, *Bull. Seismol. Soc. Am.*, *67*, 713–724.
- Lee, C., Q. Yin, R. L. Rudnick, and S. B. Jacobsen (2001), Preservation of ancient and fertile lithospheric mantle beneath the southwestern United States, *Nature*, *411*, 69–73.
- Lehmann, I. (1959), Velocities of longitudinal waves in the upper part of the Earth's mantle, *Ann. Geophys.*, *15*, 93–113.
- Leven, J. H. (1981), Upper mantle seismic anisotropy and lithospheric decoupling, *Nature*, *289*, 234–239.

- Li, A., K. M. Fischer, S. van der Lee, and M. E. Wysession (2002), Crust and upper mantle discontinuity structure beneath eastern North America, *J. Geophys. Res.*, *107*(B5), 2100, doi:10.1029/2001JB000190.
- Lipman, P. W., H. Prostka, and R. Christiansen (1971), Evolving subduction zones in the western United States, as interpreted from igneous rocks, *Science*, *174*, 821–825.
- Marshak, S., and T. Paulsen (1996), Midcontinent U.S. fault and fold zones: A legacy of Proterozoic intracratonic extensional tectonism?, *Geology*, *24*, 151–154.
- Marshak, S., K. Karlstrom, and J. M. Timmons (2000), Inversion of Proterozoic extensional faults: An explanation for the pattern of Laramide and Ancestral Rockies intracratonic deformation, United States, *Geology*, *28*, 735–738.
- McKenzie, D. (1978), Some remarks on the development of sedimentary basins, *Earth Planet. Sci. Lett.*, *40*, 25–32.
- McMillan, N. J. (1998), Temporal and spatial magmatic evolution of the Rio Grande Rift, *Field Conf. Guideb. N. M. Geol. Soc.*, *49*, 107–116.
- Mendelsohn, M. J., and G. D. Price (1997), Computer modelling of a pressure induced phase change in clinostatite pyroxenes, *Phys. Chem. Miner.*, *25*, 55–62.
- Morgan, P., W. Seager, and M. Golombek (1986), Cenozoic thermal, mechanical and tectonic evolution of the Rio Grande Rift, *J. Geophys. Res.*, *91*, 6263–6276.
- Mosher, S. (1998), Tectonic evolution of the southern Laurentian Grenville orogenic belt, *Geol. Soc. Am. Bull.*, *110*, 1357–1375.
- Olsen, K. H., G. R. Keller, and J. N. Stewart (1979), Crustal structure along the Rio Grande Rift from seismic refraction profiles, in *Rio Grande Rift: Tectonics and Magmatism*, edited by R. E. Riecker, pp. 127–143, AGU, Washington, D. C.
- Olsen, K. H., W. S. Baldrige, and J. F. Callender (1987), Rio Grande Rift: An overview, *Tectonophysics*, *143*, 119–139.
- Perry, F. V., W. S. Baldrige, and D. J. DePaolo (1988), Chemical and isotopic evidence for lithospheric thinning beneath the Rio Grande Rift, *Nature*, *332*, 432–434.
- Reed, J. C., Jr., T. T. Ball, G. L. Farmer, and W. B. Hamilton (1993), A broader view, in *The Geology of North America*, vol. C2, *Precambrian: Conterminous U. S.*, edited by J. C. Reed Jr. et al., pp. 614–622, Geol. Soc. of Am., Boulder, Colo.
- Revenaugh, J., and T. H. Jordan (1991), Mantle layering from ScS reverberations: 3. The upper mantle, *J. Geophys. Res.*, *96*, 19,781–19,810.
- Riter, J. C. A., and D. Smith (1996), Xenolith constraints on the thermal history of the mantle below the Colorado Plateau, *Geology*, *24*, 267–270.
- Roberts, D., D. Adams, and G. R. Keller (1991), A geophysical analysis of crustal structure in the Ruidoso area, *Field Conf. Guideb. N. M. Geol. Soc.*, *42*, 191–197.
- Roden, M. F., and N. Shimizu (1993), Ion microprobe analyses bearing on the composition of the upper mantle beneath the Basin and Range and Colorado Plateau provinces, *J. Geophys. Res.*, *98*, 14,091–14,108.
- Roden, M. F., and N. Shimizu (2000), Trace element abundances in mantle-derived minerals which bear on compositional complexities in the lithosphere of the Colorado Plateau, *Chem. Geol.*, *165*, 283–305.
- Roller, J. C. (1965), Crustal structure in the eastern Colorado Plateau province from seismic refraction measurements, *Bull. Seismol. Soc. Am.*, *55*, 107–119.
- Seager, W. R., and P. Morgan (1979), Rio Grande Rift in southern New Mexico, west Texas, and northern Chihuahua, in *Rio Grande Rift: Tectonics and Magmatism*, edited by R. E. Riecker, pp. 87–106, AGU, Washington, D. C.
- Selverstone, J., A. Pun, and K. C. Condie (1999), Xenolithic evidence for Proterozoic crustal evolution beneath the Colorado Plateau, *Geol. Soc. Am. Bull.*, *111*, 590–606.
- Shearer, P. M. (1991), Constraints on upper mantle discontinuities from observations of long-period reflected and converted phases, *J. Geophys. Res.*, *96*, 18,147–18,182.
- Sheehan, A. F., G. A. Abers, C. H. Jones, and A. L. Lerner-Lam (1995), Crustal thickness variations across the Colorado Rocky Mountains from teleseismic receiver functions, *J. Geophys. Res.*, *100*, 20,391–20,404.
- Sinno, Y. A., and G. R. Keller (1986), A Rayleigh wave dispersion study between El Paso, Texas, and Albuquerque, New Mexico, *J. Geophys. Res.*, *91*, 6168–6174.
- Sloss, L. L. (Ed.) (1988), Sedimentary cover, North American Craton, U.S., *The Geology of North America*, vol. D2, *Sedimentary Cover of the North American Craton: U.S.*, Geol. Soc. of Am., Boulder, Colo.
- Smith, D. (2000), Insights into the evolution of the uppermost continental mantle from xenolith localities on and near the Colorado Plateau and regional comparisons, *J. Geophys. Res.*, *105*, 16,769–16,781.
- Smith, D., D. E. Moser, J. Connelly, K. Manser, and D. Schulze (2002), U-Pb zircon ages of eclogites, garnetites, and Cenozoic rock-water reactions in Proterozoic mantle below the Colorado Plateau, *Geol. Soc. Am. Abstr. Programs*, *34*, 253.
- Stewart, S. W., and L. C. Pakiser (1962), Crustal structure in eastern New Mexico interpreted from the GNOME explosion, *Bull. Seismol. Soc. Am.*, *52*, 1017–1030.
- Topozada, T. R., and A. R. Sanford (1976), Crustal structure in central New Mexico interpretation from the Gasbuggy explosion, *Bull. Seismol. Soc. Am.*, *66*, 877–886.
- Wendlandt, E., D. J. DePaolo, and W. S. Baldrige (1993), Nd and Sr isotope chronostratigraphy of Colorado Plateau lithosphere: Implications for magmatic and tectonic underplating of the continental crust, *Earth Planet. Sci. Lett.*, *116*, 23–43.
- Wernicke, B. (1985), Uniform sense normal simple shear of the continental lithosphere, *Can. J. Earth. Sci.*, *22*, 108–125.
- West, M., J. Ni, W. S. Baldrige, D. Wilson, R. Aster, W. Gao, and S. Grand (2004), Crust and upper mantle shear wave structure of the southwest United States: Implications for rifting and support for high elevation, *J. Geophys. Res.*, *109*, B03309, doi:10.1029/2003JB002575.
- Wilson, D., and R. Aster (2005), Seismic imaging of the crust and upper mantle using regularized joint receiver functions, frequency–wave number filtering, and multimode Kirchhoff migration, *J. Geophys. Res.*, *B05305*, doi:10.1029/2004JB003430.
- Wilson, D., J. Leon, R. Aster, J. Ni, J. Schlue, S. Grand, S. Semken, S. Baldrige, and W. Gao (2002), Broadband seismic background noise at temporary seismic stations observed on a regional scale in the southwestern United States, *Bull. Seismol. Soc. Am.*, *92*, 3335–3341.
- Wilson, D., R. Aster, and the RISTRA Group (2003), Imaging crust and upper mantle seismic structure in the southwestern United States using teleseismic receiver functions, *Leading Edge*, *22*, 232–237.
- Yuan, X., J. Ni, R. Kind, J. Mechie, and E. Sandvol (1997), Lithospheric and upper mantle structure of southern Tibet from a seismological passive source experiment, *J. Geophys. Res.*, *102*, 27,491–27,500.
- Zandt, G. (2003), The southern Sierra Nevada drip and the mantle wind direction beneath the southwestern United States, *Int. Geol. Rev.*, *45*(3), 213–224.
- Zandt, G., and C. J. Ammon (1995), Continental crust composition constrained by measurements of crustal Poisson's ratio, *Nature*, *374*, 152–154.
- Zhu, L., and H. Kanamori (2000), Moho depth variation in southern California from teleseismic receiver functions, *J. Geophys. Res.*, *105*, 2969–2980.

R. Aster, Department of Earth and Environmental Science, New Mexico Institute of Mining and Technology, 801 Leroy Place, Socorro, NM 87801, USA.

W. S. Baldrige, Earth and Environmental Sciences Division, MS D462, Los Alamos National Laboratory, Los Alamos, NM 87545, USA.

W. Gao, S. Grand, and D. Wilson, Department of Geological Sciences, University of Texas at Austin, 1 University Station C1100, Austin, TX 78712, USA. (davew@geo.utexas.edu)

J. Ni and M. West, Department of Physics, MSC 3D, New Mexico State University, Las Cruces, NM 88003, USA.

S. Semken, Department of Geological Sciences, Arizona State University, Tempe, AZ 85287, USA.